Progress of Theoretical Physics, Vol. 47, No. 4, April 1972

Inclusive Reactions and Urbaryon Rearrangement Diagrams*)

Hujio NODA and Kisei KINOSHITA

Department of Physics, Kyushu University, Fukuoka

(Received October 5, 1971)

The inclusive reactions $a+b\to c+$anything are investigated on the basis of the structure of urbaryon rearrangement diagrams combined with the generalized optical theorem. The dominant production mechanism of single-particle distributions is characterized by three categories mapped onto three types of urbaryon rearrangement diagrams, respectively. The asymptotic form of each production mechanism is discussed, assuming that the structure of the effective energy dependence of hadron reaction amplitudes is specified by the rearranged urbaryon number. The overall picture for the inclusive reactions including the resonance-production region is given.

§ 1. Introduction and summary

Since the scaling behaviour concerning the structure of high energy hadron-hadron interaction was suggested by Benecke et al.[1] and Feynman,[2] inclusive reactions have attracted much attention of both theorists and experimentalists. In inclusive reactions, the intensity and momentum spectra of single-particle distributions at high energies exhibit interesting differences corresponding to the kind of the particles produced, such as shown in Fig. 1.[3] Such differences, together with the scaling behaviour in the wide range of energies,[4] may provide important clues to understand multi-particle production phenomena.

In this paper, the above features of single-particle distributions are investigated from the viewpoint that particle pro-

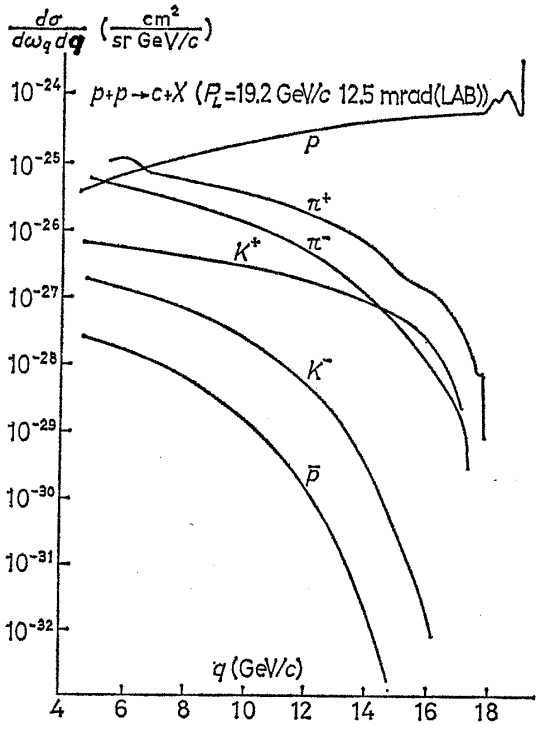

Fig. 1. Comparison of the laboratory momentum spectra for $\pi^\pm$, $K^\pm$, p and $\bar{p}$ produced at 12.5 mrad by proton-proton collisions at 19.2 GeV/c.[3]

*) Preliminary reports of this work have been published in Prog. Theor. Phys. **46** (1971), 1639, 1642.

ductions are characterized by the flow of urbaryon lines carrying internal quantum numbers among the incoming and outgoing hadrons in the reactions.*) Combined with Mueller's proposal[5] of the generalized optical theorem, the production mechanisms in terms of the flow of urbaryon lines for the process $a+b\to c+$ anything (X) are characterized by a few types of urbaryon rearrangement diagrams (URD)[6] for the amplitude $a+\bar{c}+b\to a+\bar{c}+b$. Then, the gross difference of the production rates is recognized by different types of URD characterizing the production mechanism, and the ratio of the cross sections for similar processes can be obtained by counting the coefficients of a dominant type of URD. The scaling law in the sense of Feynman[2] is easily incorporated in the URD for the $a\bar{c}b\to a\bar{c}b$ amplitudes, and the shapes of the single-particle spectra are parametrized unifiedly on the basis of URD.

Also the background part in the resonance production region can be evaluated from the scaling part obtained far inside the kinematical boundary. Thus, our approach may provide an overall picture for inclusive reactions with respect to the variety of particles and the kinematical situations.

In § 2, the dominant production mechanisms of single-particle distributions are classified into three categories, which are represented by the $D\otimes P$, $H\otimes P$ and $P\otimes P$ types of URD for the three-body→three-body amplitude.**) The variety of the intensities and shapes of the secondary particle spectra such as shown in Fig. 1 will be understood in relation to these categories. The factorization of the Pomeron coupling can be incorporated in the above types of URD. Furthermore, the $H\otimes P$ type URD provides counting relations among different processes.

The scaling behaviour in the sense of Feynman[2] and the shapes of the spectra in the scaling limit are discussed in § 3. Our basic assumption is that the structure of the effective energy dependence of the hadron reaction amplitudes is specified by the rearranged urbaryon number.[6),7] The mechanism of the flow of urbaryon lines prescribes the x-dependence of the scaling form in the asymptotic limits, where $x=2q_{\parallel}/\sqrt{s}$ with $\sqrt{s}$ the total energy and $q_{\parallel}$ the longitudinal momentum of the produced particle.

In the so-called pionization region, only the $P\otimes P$ type remains as an asymptotic contribution. On the other hand, all the three types contribute in the region of small momentum transfer, where the $D\otimes P$ type exhibits a scaling form different from the $(1-x)$-power behaviour of the other two. In other words the triple-Pomeron coupling in the $D\otimes P$ type should be disregarded, but the $D\otimes P$ type should be taken into account through single-Pomeron parametrization. The scaling forms for the $H\otimes P$ and $P\otimes P$ types correspond to an interpolation of the triple-Reggeon parametrization to the very low energy region.[8] (Our approach based on URD contrasts with the Regge phenomenology in giving gross features

*) Here we take the quark triplet for the urbaryons.

**) Typical examples of the $D\otimes P$, $H\otimes P$ and $P\otimes P$ types will be shown in Fig. 3 in the next section.

of various single-particle distributions by utilizing "rearrangement propagator", $s^{1-\gamma n_R}$, where n_R denotes the number of the rearranged urbaryon, not only non-exotic but also exotic states. We call the state of $n_R=0$ Pomeron.)

Our scheme is compared with experiment in §§ 4 and 5. As a typical data, we treat $p+p\to(p, K^{\pm}$ or $\bar{p})+X$ at 19.2 GeV/c and $K^{+}+p\to\pi^{-}+X$ at 11.8 GeV/c except kinematical boundary in § 4. The resonance production region is considered in § 5, where other types of URD, called the $D\otimes H$ and $H\otimes H$ types, are introduced since they contribute to the resonance production. They, however, do not scale in the high energy limit. The background is treated in a picture consistent with the scaling region.

In the last section, new aspects and problems in our investigation of the urbaryon line picture are discussed and comments on other approaches to inclusive reactions are given. The kinematics and notation are explained in the Appendix. The triangle plot for the Mandelstam variables and missing mass squared is explained in detail, which is convenient in visualizing the kinematics and scaling behaviour.

§ 2. Production mechanism and urbaryon rearrangement diagram

In this section we consider the inclusive reaction $a+b\to c+X$ and discuss the production mechanism for single-particle distributions on the basis of URD. In high energy hadron-hadron collision, the number of the particles produced increases and the production mechanism may become complicated. However, the flow of the urbaryon lines, which carry internal quantum numbers in collision, may be considered to characterize the reaction mechanism. In fact, when we pay attention to the flow of urbaryons, of which the produced particle c is made, we may classify the production mechanism into the following three categories:

Category (I): The particle c is the same as one of the incident particle a or b, and all the lines in the latter flow into c,

Category (II): Part of the lines in the incident particles a or b flows into c,

Category (III): None of the lines in the incident particles a and b flow into c. The produced particle c is made of urbaryons which are newly created in the collision.

Another category in which lines in c are connected with both a and b is disregarded here. Also the Iizuka rule[9] is properly considered. In Fig. 2, we illustrate these three categories.

On the basis of the generalized optical theorem and URD, we can precisely define the above three categories. As pointed by Mueller, the single-particle distribution $(\omega_q d\sigma/d\boldsymbol{q})$ of $a+b\to c+X$ is related to the discontinuity of the forward elastic three-body amplitude of $a+\bar{c}+b\to a+\bar{c}+b$ as follows:

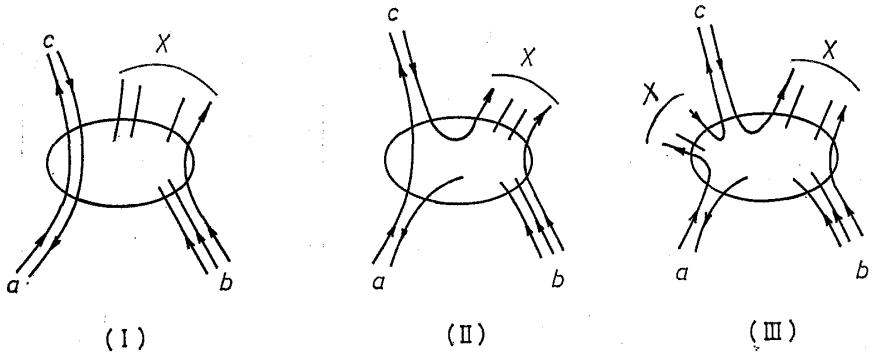

Fig. 2. Typical examples of the three categories for the urbaryon line flow in high energy hadron-hadron collision.

$$\omega_q \frac{d\sigma}{d\boldsymbol{q}} \approx \frac{1}{\sqrt{\lambda(s, m_a^2, m_b^2)}} A_3(a\bar{c}b \to a\bar{c}b),$$
$$\lambda(s, m_a^2, m_b^2) = s^2 + m_a^4 + m_b^4 - 2s(m_a^2 + m_b^2) - 2m_a^2 m_b^2, \tag{2·1}$$

where $A_3(a\bar{c}b \to a\bar{c}b)$ denotes the discontinuity in the variable $(p_a + p_b - q)^2$ obtained through an appropriate analytic continuation of the forward elastic three-body amplitude (see the Appendix about notations). The three-body amplitude is expressed as a linear sum of the URD amplitudes. The three categories are dominated by the following three types of URD:

Category (I) —— $D \otimes P$ type URD,
Category (II) —— $H \otimes P$ type URD,
Category (III) —— $P \otimes P$ type URD.

Here the notation $A \otimes P$ with $A = D$, H and P implies that, in the $a\bar{c}b \to a\bar{c}b$ amplitude, A denotes the structure of $a\bar{c} \to a\bar{c}$ part and $\otimes P$ means that $b \to b$ part is disconnected to the $a\bar{c} \to a\bar{c}$ part (the interaction between $a\bar{c}$ and b can be expressed by Pomeron exchange in some situations, as will be shown in the next section). The notation H is the well-known planer diagram,[6] and D is introduced to denote the diffraction scattering of a into c. As typical examples, we show the three types of URD for a(Meson) + b(Baryon) $\to c$(Meson) + X in the forward direction of the particle a, in Fig. 3.

When we define the forward direction of the particle a as $q_\parallel > 0$ and the backward direction of the particle a as $q_\parallel < 0$ in the center-of-mass system, we can describe the total amplitude as follows:

For $q_\parallel > 0$,

$$A_3 = F_a^c(D \otimes P) + F_a^c(H \otimes P) + F_a^c(P \otimes P), \tag{2·2}$$

and for $q_\parallel < 0$,

$$A_3 = F_b^c(D \otimes P) + F_b^c(H \otimes P) + F_b^c(P \otimes P), \tag{2·3}$$

where F_a^c and F_b^c denote the discontinuities of each URD amplitude. $F_a^c(H \otimes P)$

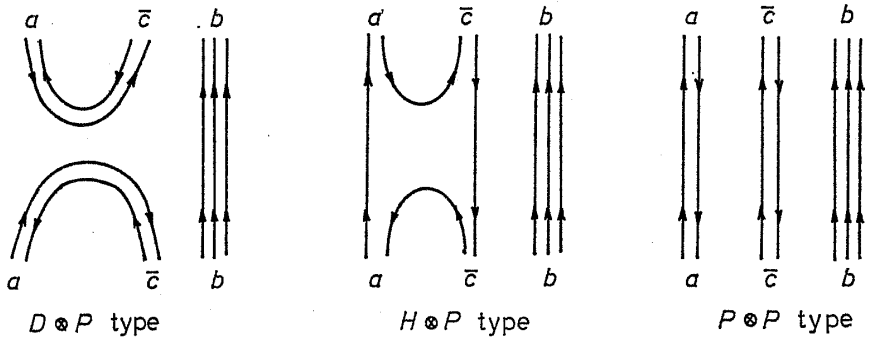

Fig. 3. Typical examples of the three types of URD ((I) $D\otimes P$ type, (II) $H\otimes P$ type and (III) $P\otimes P$ type) for the reaction $a+\bar{c}+b\to a+\bar{c}+b$.

denotes the fragmentation from the particle a and $F_b^c(H\otimes P)$ from the particle b.

For example we consider $p+p\to(p, \pi^{\pm}, K^{\pm}$ and $\bar{p})+X$. Then we can describe their amplitudes for $q_{\parallel}>0$ as follows:

$$\begin{aligned}
&A_3^p \sim F_p^p(D\otimes P)+F_p^p(H\otimes P)+F_p^p(P\otimes P),\\
&A_3^{\pi^+} \sim F_p^{\pi^+}(H\otimes P)+F_p^{\pi^+}(P\otimes P),\\
&A_3^{\pi^-} \sim F_p^{\pi^-}(H\otimes P)+F_p^{\pi^-}(P\otimes P),\\
&A_3^{K^+} \sim F_p^{K^+}(H\otimes P)+F_p^{K^+}(P\otimes P),\\
&A_3^{K^-} \sim F_p^{K^-}(P\otimes P),\\
&A_3^{\bar{p}} \sim F_p^{\bar{p}}(P\otimes P).
\end{aligned} \tag{2·4}$$

They show that the behaviour of momentum spectra of the produced particles is grouped into three classes, namely p, $(\pi^{\pm}, K^+)$ and $(K^-, \bar{p})$. As shown in Fig. 1, the experiment exhibits such behaviour. Also we may obtain the following intensity relation from experimental feature at small angle in a few tens GeV region:

$$F_a^c(D\otimes P)\gtrsim F_a^c(H\otimes P)\gtrsim F_a^c(P\otimes P). \tag{2·5}$$

By the dynamical characters of URD, we call the three categories of the production mechanism (I) diffraction mechanism, (II) fragmentation mechanism and (III) pionization-like mechanism. The mechanisms (I) and (II) are expected to contribute in the peripheral region, and the mechanism (III) in the central region.

Further, we discuss the fragmentation mechanism from the particle a to the particle c, which is defined as the $H\otimes P$ type URD. We assume the following factorization:

$$F_a^c(H\otimes P)\sim H_a^c s g_{Pb\bar{b}}, \tag{2·6}$$

where H_a^c denotes the vertex function and $g_{Pb\bar{b}}$ is the Pomeron coupling. The

vertex function $H_a{}^c$ is characterized by the H type URD. Its typical examples are shown in Fig. 4, where we denote the vertex function of the fragmentation from Meson to Meson h_{MM}, from Baryon (Meson) to Meson (Baryon) $h_{BM}(h_{M\bar{B}})$ and from Baryon to Baryon $h_{B\bar{B}}$ and $h^d_{B\bar{B}}$. In Table I, the vertex functions for the typical processes are given; the weights are calculated from the counting rule.[6),10)] Here we note that the processes $p\to\Sigma^-$ and Ξ^- are included in Table I according to our previous argument that the exotic meson states $(qq\bar{q}\bar{q})$ are considered to exist.[10)]

We examine some consequences of the factorization of Eq. (2·6) and the counting of the H type vertex function. We consider the production of a strange particle. In this case we assume the $H\otimes P$ type dominance, because of the small

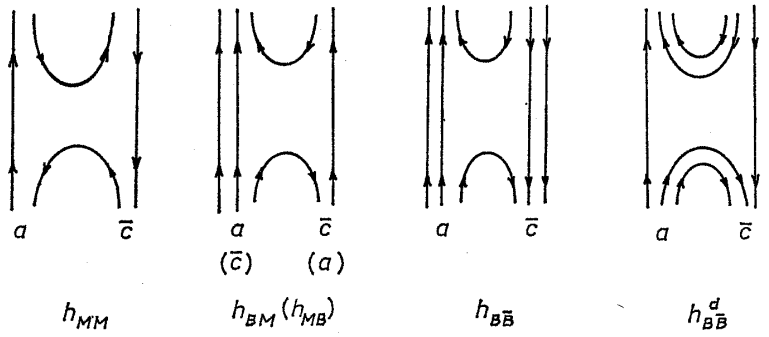

Fig. 4. Typical H type URD to characterize the fragmentation mechanism from the particle a to the particle c.

Table I. Vertex function $H_a{}^c$ mapped on the H type URD.

$a\to c$	$H_a{}^c$	$a\to c$	$H_a{}^c$	$a\to c$	$H_a{}^c$
$p\to p$	$5h^d_{B\bar{B}}+5h_{B\bar{B}}$	$\pi^+\to K^0$	0	$K^-\to\Sigma^-$	$h_{M\bar{B}}$
n	$h^d_{B\bar{B}}+4h_{B\bar{B}}$	$\bar{K}^0$	h_{MM}	Ξ^-	$2h_{M\bar{B}}$
Λ	$3/2h^d_{B\bar{B}}+3h_{B\bar{B}}$	$\pi^-\to\pi^+$	0	$\bar{\Lambda}$	$h_{M\bar{B}}$
Σ^+	$h^d_{B\bar{B}}+4h_{B\bar{B}}$	π^-	$2h_{MM}$	$\bar{\Xi}^+$	0
Σ^0	$1/2h^d_{B\bar{B}}+3h_{B\bar{B}}$	K^+	0	$K^+\to K^+$	$2h_{MM}$
Σ^-	$2h_{B\bar{B}}$	K^-	h_{MM}	K^-	0
Ξ^-	$h_{B\bar{B}}$	K^0	h_{MM}	K^0	h_{MM}
Ξ^0	$2h_{B\bar{B}}$	$\bar{K}^0$	0	$\bar{K}^0$	0
π^+	$2h_{BM}$	$K^-\to K^-$	$2h_{MM}$	π^-	0
π^-	h_{BM}	K^+	0	π^+	h_{MM}
K^+	$2h_{BM}$	K^0	0	p	$2h_{M\bar{B}}$
K^-	0	$\bar{K}^0$	h_{MM}	Λ	$h_{M\bar{B}}$
K^0	h_{BM}	π^+	0	Σ^+	$2h_{M\bar{B}}$
$\bar{K}^0$	0	π^-	h_{MM}	Σ^-	0
$\pi^+\to\pi^+$	$2h_{MM}$	p	0	Ξ^-	0
π^-	0	Λ	$h_{M\bar{B}}$	$\bar{p}$	0
K^+	h_{MM}	Σ^0	$h_{M\bar{B}}$	$\bar{\Lambda}$	$h_{M\bar{B}}$
K^-	0	Σ^+	$h_{M\bar{B}}$	$\bar{\Xi}^+$	$2h_{M\bar{B}}$

contribution of the $P\otimes P$ type. Therefore, we may calculate the production cross section as follows:

$$\sigma(ab\to cX)=\int d\boldsymbol{q}\frac{d\sigma(ab\to cX)}{d\boldsymbol{q}}$$
$$\simeq\int d\boldsymbol{q}\{g_{Pb\bar{b}}H_a{}^c+g_{Pa\bar{a}}H_b{}^c\}\frac{1}{\omega_q}. \qquad (2\cdot7)$$

For example, we treat the production ratio of $K^+p\to\bar{\Xi}^+X$ and $K^+p\to\Xi^-X$. Then from Eq. (2·7) we obtain

$$R\equiv\frac{\sigma(K^+p\to\bar{\Xi}^+X)}{\sigma(K^+p\to\Xi^-X)}\simeq\frac{g_{P\bar{p}\bar{p}}\int d\boldsymbol{q}H_{K^+}^{\bar{\Xi}^+}/\omega_q}{g_{PK^+K^-}\int d\boldsymbol{q}H_p{}^{\Xi^-}/\omega_q}.$$

From Table I, we have $H_{K^+}^{\bar{\Xi}^+}=2h_{M\bar{B}}$ and $H_p{}^{\Xi^-}=h_{B\bar{B}}$. Thus,

$$R\simeq\frac{2g_{P\bar{p}\bar{p}}\int d\boldsymbol{q}h_{M\bar{B}}/\omega_q}{g_{PK^+K^-}\int d\boldsymbol{q}h_{B\bar{B}}/\omega_q}.$$

If we further assume the approximate equality of the vertex functions,[10),11)] namely $\int d\boldsymbol{q}h_{M\bar{B}}/\omega_q\simeq\int d\boldsymbol{q}h_{B\bar{B}}/\omega_q$, we obtain

$$R\simeq\frac{2g_{P\bar{p}\bar{p}}}{g_{PK^+K^-}}\simeq\frac{2\sigma_T(p\bar{p})}{\sigma_T(K^+p)}\simeq4.4.$$

This result is in good agreement with the recent experimental result ($R_{\text{exp}}\simeq4$ at $P_L\simeq12.7$ GeV/c).[12)] Similarly we have the following results:

Ratio	Theory	Experiment	
$\frac{\sigma(K^+p\to\bar{\Lambda}X)}{\sigma(K^+p\to\Lambda X)}$	0.37	0.4	at $P_L\simeq12.7$ GeV/c,[12)]
$\frac{\sigma(pp\to\Sigma^+X)}{\sigma(pp\to\Sigma^-X)}$	2.5	4.0 ± 0.9	at $P_L\simeq24.5$ GeV/c,[13)]
$\frac{\sigma(\pi^-p\to\Sigma^+X)}{\sigma(\pi^-p\to\Sigma^-X)}$	1.0	1.3 ± 0.3	at $P_L\simeq16$ GeV/c.[13)]

These results demonstrate that the factorization and the counting picture work very well at the asymptotic region.

§ 3. Asymptotic forms of single-particle distributions

We have discussed the production mechanism for inclusive reactions on the basis of URD in the previous section. In this section we study the asymptotic distribution of single particle for each production mechanism. In particular we pay attention to the x-dependence of single-particle distributions. Our basic assumption is that the structure of the effective energy dependence of hadron reaction amplitudes is specified by the rearranged urbaryon number. This picture

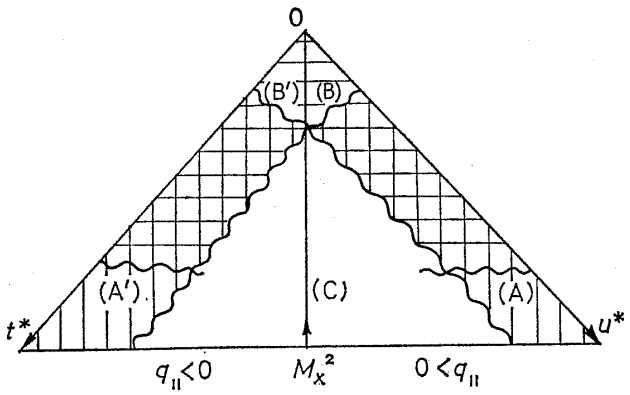

Fig. 5. The kinematical regions on the triangle plot.

is very useful in analyzing complicated hadron phenomena.

Invariant variables t^*, u^* and M_X^2 introduced in the Appendix are convenient for picking out the essential part of the asymptotic distributions. (Details of the kinematics and our notation are explained in the Appendix.) In the forward production of the particle c with small t^*, there may exist two possibilities of parametrization according as whether (A) the $a+\bar{c}\to a+\bar{c}$ part of the $a+\bar{c}+b\to a+\bar{c}+b$ amplitude should be treated as single vertex, or (B) initial $a\bar{c}$ turns into single sub-system and then interact with b. On the other hand, the case (C) in which both t^* and u^* are large should be parametrized differently. For the backward production, we have cases (A′) and (B′) by interchanging the roles of a and b.

We consider the asymptotic distributions in the following kinematical regions for each case as shown in Fig. 5:

(A) t^* small fixed, u^* large and u^*/s fixed,
(B) t^* small fixed, M_X^2 large and M_X^2/s fixed,*)
(C) both t^* and u^* large, and t^*u^*/s fixed,
(A′) u^* small fixed, t^* large and t^*/s fixed,
(B′) u^* small fixed, M_X^2 large and M_X^2/s fixed.

These situations may be schematically described by the tree-like diagrams shown in Fig. 6. We may evaluate the contributions of each URD in these situations by deforming them to the corresponding forms in Fig. 6, conserving their line topology. In Fig. 6, n_i denotes the number of rearranged urbaryons in each sections.

From our basic assumption, we take following parametrizations of the URD amplitudes for each situation:

$$A_3(t^*, u^*; s) = \xi_{a\bar{c}}(u^*)^{1-\gamma n_3} g_{3b\bar{b}} \qquad \text{for (A)},$$

$$A_3(t^*, u^*; s) = \eta_{a\bar{c}} \left(\frac{s}{M_X^2}\right)^{1-\gamma n_1} \left(\frac{s}{M_X^2}\right)^{1-\gamma n_2} (M_X^2)^{1-\gamma n_3} g_{3b\bar{b}} \qquad \text{for (B)},$$

$$A_3(t^*, u^*; s) = g_{4a\bar{a}}(t^*)^{1-\gamma n_4} \zeta_c (u^*)^{1-\gamma n_3} g_{3b\bar{b}} \qquad \text{for (C)}, \tag{3·1}$$

where g is the forward coupling constant, and ξ, η and ζ are vertex functions containing t^* or $q_\perp^2$ dependence. In these parametrizations, we have adopted from

*) Here we do not impose the restriction $M_X^2 \ll s$, in contrast to the Regge pole model near the kinematical boundary.

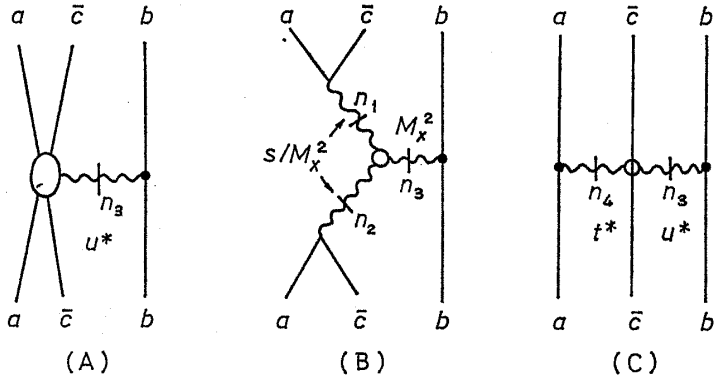

Fig. 6. The deformation patterns of each type URD corresponding to the kinematical regions (A), (B) and (C), where n_i denotes the number of the rearranged urbaryons in each section.

our basic assumption the rearranged form s^{1-rn_R} for the energy dependence, instead of the Regge form $s^{\alpha(t)}$. The value of γ is expected to be $0.5\sim0.7$.*) The above forms are sufficient to study the scaling law and the asymptotic forms for the variable x. Then the scaling law implies that the single-particle distribution $(\omega_q d\sigma/d\boldsymbol{q})$ becomes energy independent at very high energies. By using the relations for large s,

$$\frac{u^*}{s}\simeq\frac{x+\bar{x}}{2}, \qquad \frac{M_X^2}{s}\simeq 1-\bar{x}, \tag{3·2}$$

we can easily see the scaling conditions and scaling forms of $\rho\equiv\omega_q(d\sigma/d\boldsymbol{q})\simeq A_3/s$. For small t^*, the scaling condition is $n_3=0$, which is satisfied for the three types of URD adopted in our approach, since we have

$$\begin{aligned}\rho&\propto\frac{x+\bar{x}}{2}(u^*)^{-rn_3} \qquad \text{for (A)},\\ \rho&\propto(1-\bar{x})^{r(n_1+n_2)-1}(M_X^2)^{-rn_3} \qquad \text{for (B)}.\end{aligned} \tag{3·3}$$

On the other hand, only the $P\otimes P$ type exhibits scaling at large t^* and u^*, since we have

$$\rho\simeq\zeta_c\cdot(q_\perp^2+m_c^2)\,(t^*)^{-rn_4}(u^*)^{-rn_3}. \tag{3·4}$$

If ζ_c depends on $q_\perp^2$ only, the scaling contribution at large $q_\perp^2$ does not exhibit x-dependence. Thus, we may treat all the scaling contributions in terms of the three types of URD, i.e., $D\otimes P$, $H\otimes P$ and $P\otimes P$. The x-dependence of single-particle distributions of each type in each situation in the scaling limit is summarized as follows:

Case	$D\otimes P$ type	$H\otimes P$ type	$P\otimes P$ type
(A)	x	x	x
(B)	$(1-x)^{-1}$	$(1-x)^{r(n_1+n_2)-1}$	$(1-x)^{r(n_1+n_2)-1}$
(C)	no scaling	no scaling	constant.

*) The value of γ obtained in recent analysis[14] is $0.5\sim0.7$.

The form (A) is proportional to x and (B) form has the $(1-x)$ power behaviour, while the (C) form does not depend on x because $t^*u^*/s \simeq q_\perp^2 + m_c^2$.

The dominant form for each type in small t^* will be determined phenomenologically. It is to be noted that the $(1-x)^{-1}$ behaviour of the $D\otimes P$ type is undesirable because it increases rapidly as $x\to 1$, while the (A) form is admittable. In fact it will be shown in § 4 that the $D\otimes P$ type exhibits the (A) form for $pp\to pX$. On the other hand, the $H\otimes P$ type can be described by the (B) form, as indicated by the larger contributions in the reactions $pp\to\pi^\pm X$, K^+X. In our model the $P\otimes P$ type contributes not only in the region (C), but also in the region of small t^* or u^*, contrary to the Regge pole approach without exotic trajectory or Regge-cut. Phenomenologically the (B) form of the $P\otimes P$ type is very important for the reactions $pp\to K^-X$, $pp\to\bar{p}X$, and $K^+p\to\pi^-X$, as will be shown in the next section.

The parametrization adopted for (B) corresponds to the triple-Reggeon form which has been considered under another condition $s/M_X^2 \gg 1$, i.e., $x \simeq 1$.[8] However, we will not restrict ourselves to the region of the kinematical boundary, because we do not assume the leading pole dominance. The value of γ is somewhat large, when we fit down to $x \simeq 0$. We note that the scaling form in the region (B) is more precisely described by the $(1-\bar{x})$ power form. This correction is important to understand the behaviour at $x \simeq 0$ and somewhat large $q_\perp$ (see § 4).

Finally we briefly discuss the structure of the vertex functions ξ, η and ζ. If we assume that at very high energies the separability of the longitudinal and transverse momenta is realized very well, the vertex function becomes dependent only on $q_\perp$.*) Therefore we assume the following form for the vertex function:

$$(\text{vertex functions } \xi,\ \eta \text{ and } \zeta) \propto \exp(-a(q_\perp^2 + m_c^2)), \qquad (3\cdot 5)$$

where a is a parameter.

§ 4. Comparison with experiment

We have discussed the asymptotic behaviour of single-particle distributions. In this section we compare our model with experiments. We study the inclusive reactions $pp\to pX$, $K^\pm X$ and $\bar{p}X$ at $P_L = 19.2$ GeV/c[3] and $K^+p\to\pi^-X$ at $P_L = 11.8$ GeV/c.[15] On the basis of the results in § 3 we assume the following asymptotic distribution for each URD:

For $q_\parallel > 0$,

$$\rho(D\otimes P) \sim g_{Pb\bar{b}} d_{a\bar{c}} \exp(-a_D(q_\perp^2 + m_c^2)) \left(\frac{x+\bar{x}}{2}\right) \qquad \text{for } D\otimes P \text{ type,}$$

*) Strictly speaking, the factorization of the $q_\parallel$ and $q_\perp$ dependences is fulfilled only approximately in the region of ten GeV. On this point, see ii) in § 5.

$$\rho(H\otimes P)\sim g_{Pb\bar{b}}h_{a\bar{c}}\exp(-a_H(q_\perp^2+m_c^2))(1-\bar{x})^{2\gamma n_R-1} \quad \text{for } H\otimes P \text{ type},$$
$$\rho(P\otimes P)\sim g_{Pb\bar{b}}c_{a\bar{c}}\exp(-a_P(q_\perp^2+m_c^2))(1-\bar{x})^{2\gamma n_R-1} \quad \text{for } P\otimes P \text{ type}, \tag{4·1}$$

where $n_1=n_2=n_R$ and a_D, a_H, a_P and γ are free parameters. Also $d_{a\bar{c}}$, $h_{a\bar{c}}$ and $c_{a\bar{c}}$ denote the vertex constants.

(i) $pp\to cX$ First we consider $pp\to cX$ at $P_L=19.2$ GeV/c. The experiment on $d\sigma/d\boldsymbol{q}$ for $pp\to pX$ exhibits the constant $q_\parallel$ dependence at small $q_\perp$ (see Fig. 7). This behaviour can be regarded as that of the case (A) of the $D\otimes P$ type. Therefore, when we use $x=2q_\parallel/\sqrt{s}$ and $\bar{x}=2\omega_q/\sqrt{s}$, we may parametrize the cross section as follows:

$$\frac{d\sigma}{d\boldsymbol{q}}(pp\to pX)\sim\frac{g_{Pp\bar{p}}}{\omega_q}\left\{d_{p\bar{p}}\exp(-a_D(q_\perp^2+m_N^2))\left(\frac{\omega_q+q_\parallel}{\sqrt{s}}\right)\right.$$
$$\left.+h_{p\bar{p}}\exp(-a_H(q_\perp^2+m_N^2))\left(1-\frac{2\omega_q}{\sqrt{s}}\right)^{4\gamma-1}\right\}. \tag{4·2}$$

The second term is the contribution from the $h^d_{B\bar{B}}$ fragmentation mechanism ($n_R=2$) and the other contributions are neglected according to the intensity relation Eq. (2·5). The result is shown in Fig. 7. The fit to the experiment exhibits that at small $q_\perp$ the $D\otimes P$ type is dominant and at large $q_\perp$ the $H\otimes P$ type is dominant. In the next section we discuss that this feature continues to the resonance production region.

We treat $pp\to K^+X$, which is considered to be dominated by the $H\otimes P$ type ($n_R=3$). Therefore we can parametrize as

$$\frac{d\sigma}{d\boldsymbol{q}}(pp\to K^+X)\sim\frac{g_{Pp\bar{p}}}{\omega_q}\left\{h_{pK^+}\exp(-a_H(q_\perp^2+m_K^2))\left(1-\frac{2\omega_q}{\sqrt{s}}\right)^{6\gamma-1}\right\}. \tag{4·3}$$

The fit is in good agreement with experiment, as shown in Fig. 8.

Table II. Parameters a and γ for $pp\to cX$ (eyeball fit).

reaction	type	a (GeV^{-2})	γ
$pp\to pX$	$D\otimes P$	$a_D=6.9$	—
	$H\otimes P$	$a_H=2.3$	0.50
$pp\to K^+X$	$H\otimes P$	$a_H=4.2$	0.67
$pp\to K^-X$	$P\otimes P$	$a_P=4.2$	0.70
$pp\to\bar{p}X$	$P\otimes P$	$a_P=4.2$	0.67

Similarly, the reactions $pp\to K^-X$ and $\bar{p}X$ have only the contribution from the $P\otimes P$ type. The rearranged number n_R is 5 for $pp\to K^-X$ and 6 for $pp\to\bar{p}X$. The fits are shown in Fig. 9 and Fig. 10. The values of the parameters a and γ used in each reaction are summarized in Table II. It is to be noted that the

value of a_D is larger than the other values a_H and a_P. This feature is similar to the relation of the slopes between the diffraction and the non-diffraction. Also the value of γ is $0.5\sim0.7$, which is consistent with the value estimated from the energy dependence of two- and multi-body production cross sections.[14]

(ii) $K^+p\to\pi^-X$ We consider $K^+p\to\pi^-X$ at $P_L=11.8\,\mathrm{GeV}/c$. In particular we pay attention to the forward-backward asymmetry of the x-dependence and

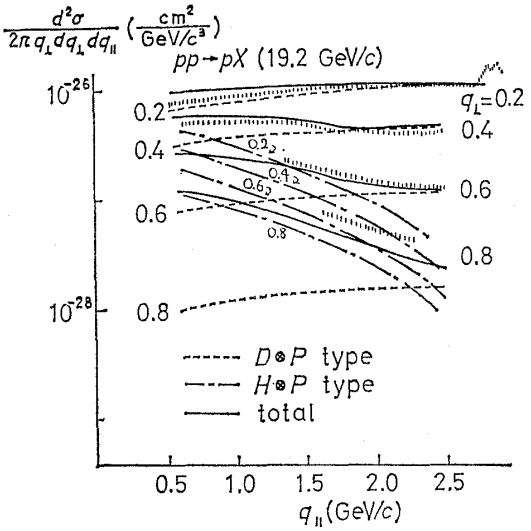

Fig. 7. The $q_\parallel$ dependence for fixed values of $q_\perp$ in the reaction $pp\to pX$ at 19.2 GeV/c from data of Ref. 3). The solid lines are results of our model.

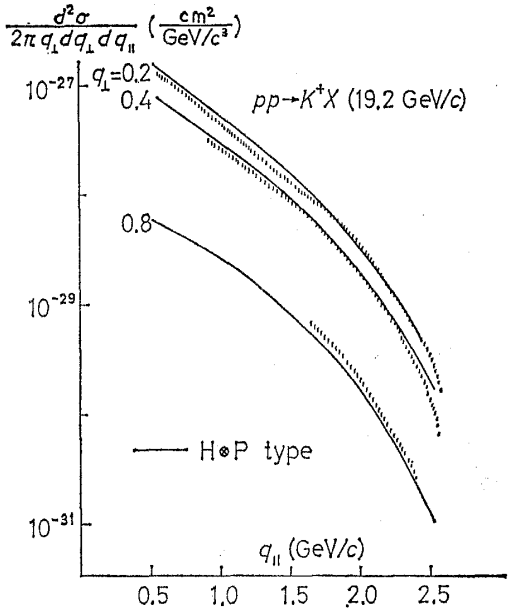

Fig. 8. The same as Fig. 7 for the reaction $pp\to K^+X$.

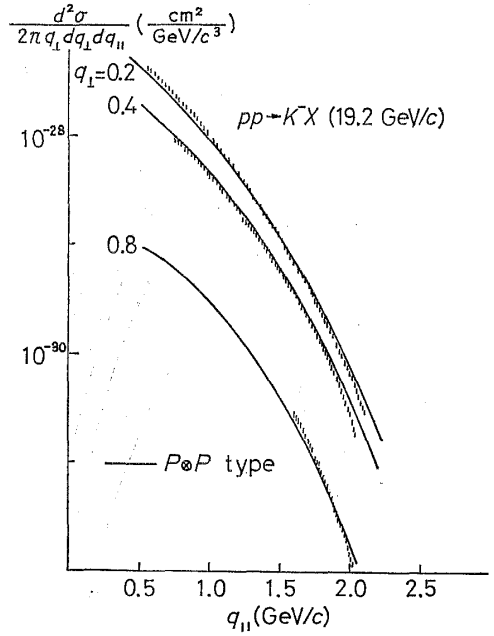

Fig. 9. The same as Fig. 7 for the reaction $pp\to K^-X$.

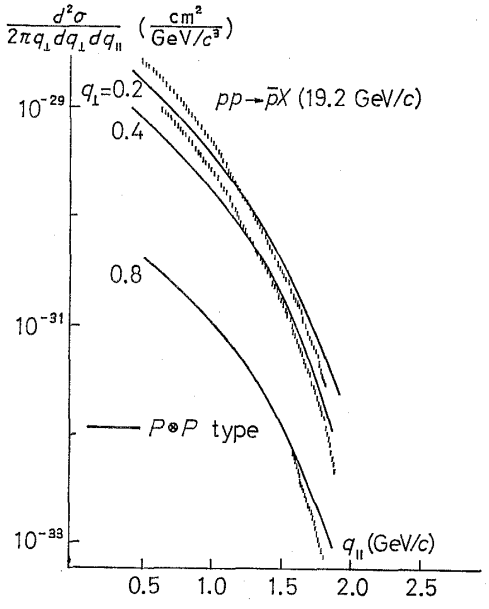

Fig. 10. The same as Fig. 7 for the reaction $pp\to\bar{p}X$.

the behaviour near $x\simeq 0$. Though for $x<0$ this reaction has the contribution from the $H\otimes P$ type as the fragmentation of proton, this contribution may be considered to be small. So we assume the $P\otimes P$ type dominance for this process. We can parametrize the cross section as follows:

$$\omega_q \frac{d\sigma}{d\boldsymbol{q}} \sim g_{Pp\bar{p}}\{c_{K^+\pi^+}\exp(-a_P{}^+(q_\perp^2+m_\pi{}^2))(1-\bar{x})^{8\gamma^+-1}\}, \quad \text{for } x>0 \tag{4·4}$$

$$\omega_q \frac{d\sigma}{d\boldsymbol{q}} \sim g_{PK^+K^-}\{c_{p\pi^+}\exp(-a_P{}^-(q_\perp^2+m_\pi{}^2))(1-\bar{x})^{10\gamma^--1}\} \quad \text{for } x<0\,. \tag{4·5}$$

The fit is shown in Fig. 11. The parameters used are

$$a_P{}^+=4.0\,(\mathrm{GeV}/c)^{-2}, \qquad \gamma^+=0.5 \qquad \text{for } x>0\,,$$

$$a_P{}^-=3.0\,(\mathrm{GeV}/c)^{-2}, \qquad \gamma^-=0.6 \qquad \text{for } x<0\,.$$

Also the $q_\perp^2$ dependence of the asymptotic distribution at the fixed x is shown in Fig. 12.

In our model the forward-backward asymmetry is understood by the difference of the rearranged urbaryon number ($n_R=4$ for $x>0$ and $n_R=5$ for $x<0$). The distributions with small fixed values of $q_\perp$ show sharp peaking near $x\simeq 0$, but the distributions at larger fixed values of $q_\perp$ are rounded near $x\simeq 0$ in contradiction to the factorization hypothesis of $q_\perp$ and x. This behaviour is explained by the $(1-\bar{x})$ dependence of the asymptotic form instead of $(1-x)$ form. Therefore it may be considered that the separability of $q_\perp^2$ and $\bar{x}$ is very good for the (B) form.

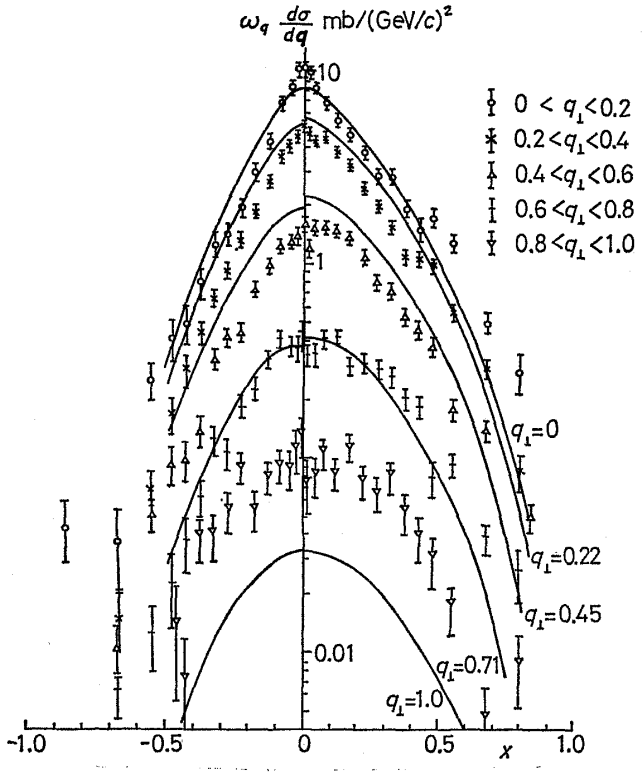

Fig. 11. The x-dependence of the π^- spectra for fixed values of $q_\perp$ produced in K^+p collisions at 11.8 GeV/c.[15] The solid lines are obtained from our model through eyeball fit.

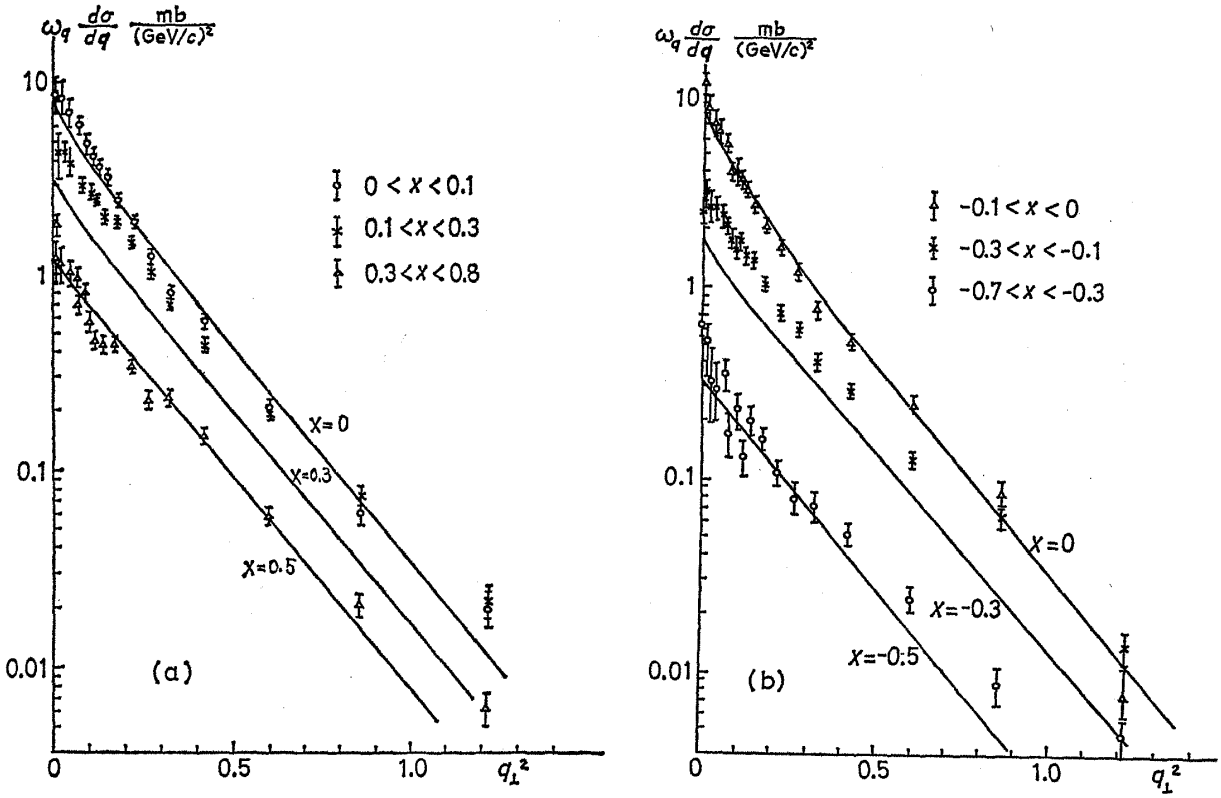

Fig. 12. The $q_\perp{}^2$ dependence for fixed values of x in the same reaction as Fig. 11. a) and b) for $x>0$ and $x<0$, respectively.

§ 5. The structure of the production mechanism in the resonance-production region

On the basis of the analysis in § 4, we consider the inclusive reaction $a+b \to a+X$ in the resonance-production region ($M_X{}^2 \ll s$). The structure of the production mechanism in this region is divided into the background part and resonance part. The former part is described by the scaling forms discussed so far. It is characterized by the $D\otimes P$ and $H\otimes P$ types. On the other hand the latter part is characterized by two new types of URD, namely $D\otimes H$ and $H\otimes H$ types, which are shown in Fig. 13. They do not exhibit the scaling behaviour in the asymptotic limit.

First we discuss the background part. In the resonance-production region, we obtain the following form for the $D\otimes P$ type from Eq. (4·1):

$$\frac{d\sigma}{dt^* dM_X} \propto \frac{M_X}{s}\left(1-\frac{M_X{}^2}{s}\right). \tag{5·1}$$

Also similarly for the $H\otimes P$ type we obtain

$$\frac{d\sigma}{dt^* dM_X} \propto \frac{M_X}{s}\left(\frac{M_X{}^2}{s}\right)^{2\gamma n_R - 1}. \tag{5·2}$$

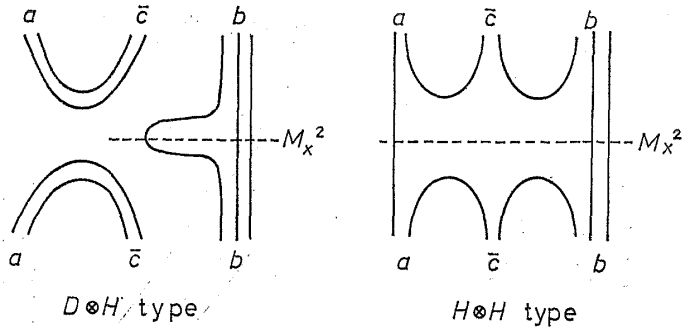

Fig. 13. Typical examples of urbaryon rearrangement diagrams to be considered near the kinematical boundary, the $D\otimes H$ and $H\otimes H$ types.

When $\gamma\simeq 0.5$ and $n_R=2$, we have $d\sigma/dt^*dM_X\propto(1/s^2)M_X^3$. It is to be noted that the background forms mainly exhibit the M_X-power behaviour and have the energy dependence. These features are in good agreement with recent experiments.[16]

Second we discuss the resonance parts. The semi-local average of the resonance parts behave as follows:

$$\frac{d\sigma}{dt^*dM_X}\propto\frac{1}{M_X^3}(M_X^2)^{1-2\gamma} \qquad \text{for } D\otimes H \text{ type}, \tag{5·3}$$

$$\frac{d\sigma}{dt^*dM_X}\propto\frac{1}{s^{4\gamma}}(M_X)^{2\gamma-1} \qquad \text{for } H\otimes H \text{ type}, \tag{5·4}$$

where we assume the (B) form for both $D\otimes H$ and $H\otimes H$ types. Also we may write the contribution of $D\otimes H$ type as follows:

$$\frac{d\sigma}{dt^*dM_X}\propto\sum_i\frac{1}{M_X^3}\,\mathrm{Im}\,(\mathrm{Res.})_i\propto\sum_i\frac{\beta_i\Gamma_i}{(M_X-M_i)^2+(\Gamma_i/2)^2},$$

where M_i and Γ_i are the mass and width of the i-th resonance, respectively, and β_i is a coefficient.

The $D\otimes H$ type exhibits the constant resonance behaviour (no s-dependence) and the $H\otimes H$ type has the s-dependence. Therefore it is expected that at high energies bumps of the nucleon resonances with the isospin 1/2 survive while Δ_{33} resonance bump disappears. This tendency is in agreement with the experimental feature[17] as shown in Figs. 14 and 15.

Now we treat the reaction $\pi^-p\to\pi^-X$. In Figs. 14 and 15, the contribution of the background parts is shown at $P_L=8$ GeV/c and $P_L=16$ GeV/c.[17] From Eqs. (5·1) and (5·2), we put

$$\frac{d\sigma}{dtdM_X}\sim d\frac{M_X}{s}\left(1-\frac{M_X^2}{s}\right) \qquad \text{for } 0.06<|t|<0.10$$

and

$$\frac{d\sigma}{dtdM_X}\sim d'\frac{M_X}{s}\left(1-\frac{M_X^2}{s}\right)+h\left(\frac{M_X^3}{s^2}\right) \qquad \text{for } 0.58<|t|<0.76,$$

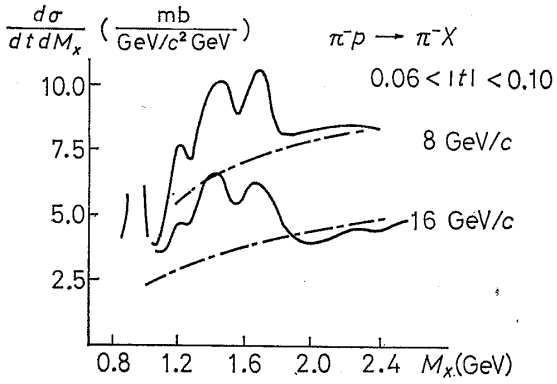

Fig. 14. The missing mass distributions for the reaction $\pi^-p\to\pi^-X$ at 8 and 16 GeV/c for $0.06<|t|<0.10$.[17] The dash-dotted lines show the background contributions from the $D\otimes P$ type in our model.

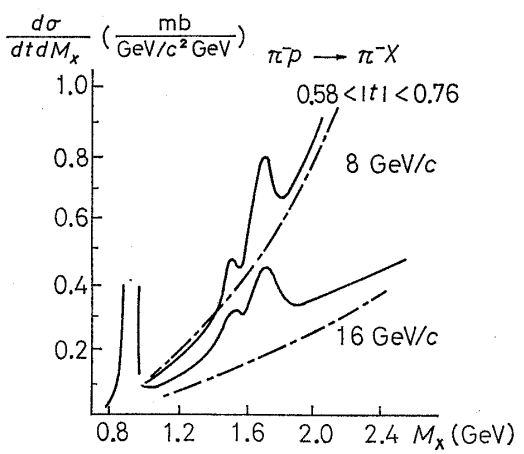

Fig. 15. The same as Fig. 14 for $0.58<|t|<0.76$. The dash-dotted lines show the background contributions from the $D\otimes P$ and $H\otimes P$ types in our model.

where the parameters d, d' and h are evaluated from experiment as $d=85$ mb/(GeV/c)^2, $d'=1$ mb/(GeV/c)^2 and $h=22$ mb/(GeV/c)^2. (Also the experimental data of $pp\to pX$ shows a similar structure to one of $\pi^-p\to\pi^-X$.[18])

At small $|t|$ the $D\otimes P$ type is dominant and at large $|t|$ the $H\otimes P$ type is dominant. The remaining bumps are explained by the resonance contributions from the $D\otimes H$ and $H\otimes H$ types. Thus we conclude that the $D\otimes P$ type exhibits the (A) form and not the (B) form which is the triple-Pomeron coupling form.

§ 6. Discussion

(1) Recently, J. Wang and L. Wang[19] pointed out that the triple Pomeron coupling is extremely small and asserted that the background part of the resonance production cannot be produced diffractively, from the analysis of the background in the resonance-production region. This, however, does not imply that the $D\otimes P$ type is not important but that the $D\otimes P$ type do not exhibit the (B) form, as pointed out in § 5. Our analysis finds that the $D\otimes P$ type exhibits the (A) form (single Pomeron parametrization) and contributes to the background in the missing mass region at small $|t|$. Also the triple Reggeon form is included in the study of the reaction $pp\to pX$ and others from the multiperipheral model of Caneschi and Pignotti,[20] but the single Reggeon form is not included in it. Therefore their picture is also different from ours in this respect. We stress the importance of the $D\otimes P$ type in the production mechanism of single-particle distributions. It remains as an open question why the D-parts in the $D\otimes P$ and $D\otimes H$ types require different treatments.

(2) We have obtained the result that the $H\otimes P$ type is characterized by the following asymptotic form:

$$\rho(H\otimes P)\propto(1-\bar{x})^{2\gamma n_R-1}.$$

Therefore, the scaling form of the $H\otimes P$ type may be grouped into several classes according to the values of n_R. For example, particles Σ^+, n, Λ and Σ^0 are expected to show different momentum spectra from particles Σ^-, Ξ^- and Ξ^0 in inclusive reactions $pp\to cX$, because the rearranged urbaryon number n_R of the former and the latter is 2 and 4, respectively. Further experiments and recompilations of the existing data for the neutron and strange baryon spectra are very desirable in order to check our scheme.

(3) We discuss the inclusive exotic processes ($pp\to\bar{K}X$, $pp\to\bar{p}X$, $K^+p\to\bar{K}X$, etc.), which are characterized only by the $P\otimes P$ type. If we treat these processes according to Mueller's Regge analysis,[5] these single-particle distributions have no x-dependence because of the two-Pomeron form (the (C) form). However, as seen in § 4, the experiments show the $(1-\bar{x})$ power dependence. Thus, the Regge analysis without exotic trajectories or Regge-cut faces the difficulty.

On the other hand, our model may overcome this difficulty by introducing exotic states, which are considered to be the dual part of the Pomeron. These exotic states appear directly in the two-body reactions $p\bar{p}\to\Omega^-\bar{\Omega}^+$ or $\phi\bar{\phi}$. At the present stage, we know few properties about these states, but we wish to stress the importance of them.

We demonstrate our model for the K^-/π^- and $\bar{p}/\pi^-$ ratios in pp collisions at $E_0\simeq 35$, 43, 52 and 70 GeV.[21] If we assume the dominance of the $H\otimes P$ type for $pp\to\pi^-X$ at the angle $\theta\simeq 0$, we simply obtain the following production ratios from our model:

$$R_{\mathrm{I}}=\frac{\rho(pp\to K^-X)}{\rho(pp\to\pi^-X)}\propto\frac{(1-x)^{10\gamma-1}}{(1-x)^{6\gamma-1}}=(1-x)^{4\gamma},$$

$$R_{\mathrm{II}}=\frac{\rho(pp\to\bar{p}X)}{\rho(pp\to\pi^-X)}\propto\frac{(1-x)^{12\gamma-1}}{(1-x)^{6\gamma-1}}=(1-x)^{6\gamma}.$$

Comparison of our predictions with experiments is shown in Fig. 16, where we put $\gamma\simeq 0.5$. The fit is in reasonable agreement with experiments.

In the multiperipheral model, these inclusive exotic processes are analyzed by the three vertex diagram.[20),22] The relation of our model to this model remains as an important problem.

(4) An interesting explanation was proposed on the forward-backward asymmetry in $K^+p\to\pi^-X$ from the standpoint of the quark frame.[23] But, when we treat a process which is not free from the "leading-particle" effects in terms of this picture, the problem is more complicated. By our model, the forward-backward asymmetry in meson-baryon collisions is explained by the differences of the production mechanism and the rearranged urbaryon number in forward and backward directions, as seen in § 4. In particular, we consider $K^-p\to\bar{K}^0X$ for example. Then both $H\otimes P$ ($n_R=2$) and $P\otimes P$ ($n_R=4$) types contribute to the forward di-

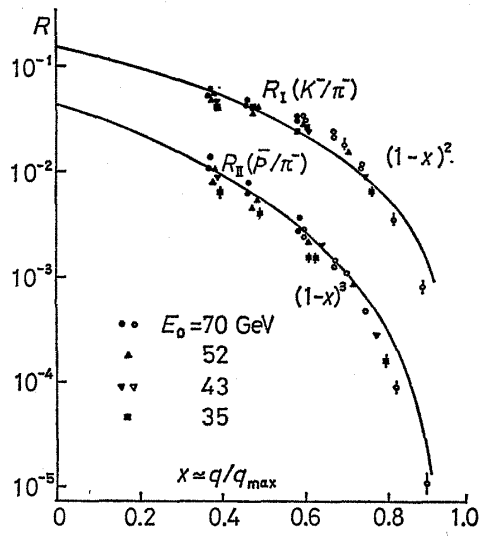

Fig. 16. Production ratio in p-p collisions as a function of $x \cong q/q_{max}$. Data are from Ref. 21). The solid lines are obtained from our model.

rection, while only the $P \otimes P$ ($n_R=5$) type contributes to the backward direction. Therefore our model qualitatively predicts the following asymmetry:

$$\rho^+ \propto (1-x) \quad \text{for } x>0,$$

$$\rho^- \propto (1-|x|)^4 \quad \text{for } x<0,$$

where $\gamma \simeq 0.5$. The recent experiment[24] exhibits the above tendency. On the other hand, it is difficult to recognize in the quark-frame approach the qualitative difference between the single-particle distributions of $K^-p \to \bar{K}^0 X$ and $K^+p \to \pi^- X$.

(5) The single-particle distribution in photon-hadron reaction was discussed in the hadron fragmentation region.[25] Much more interesting may be the fragmentation mechanism of photon (or virtual one) into hadrons, which may not be substituted for other reactions. We expect that the two-arm experiments for $e+p \to e+$hadron$+$anything give important clues in this direction. Also the relation of the recent analysis for $e+p \to e+$anything[26] to our result on the $D \otimes P$ type for $\pi^- + p \to \pi^- +$anything is very interesting; in $e+p \to e+$anything the Pomeron contribution is very small, compared with those of the vector and the tensor trajectories. The comparison of highly inelastic p-p and e-p scatterings by Allaby et al.[27] showed that for $M_X \lesssim 3.5$ GeV the structure functions for inelastic e-p and p-p scatterings look very similar in shape, but for $M_X \gtrsim 3.5$ GeV two structure functions exhibit different behaviour. This feature may be explained from the difference of the background part owing to the fragmentation of incident particle.

Acknowledgements

The authors would like to express their gratitude to Professor S. Otsuki, Professor M. Uehara and other members of their institute for valuable discussions and encouragements. One of the authors (H.N.) is also grateful for a stimulating discussions with Dr. S. Kagiyama, Dr. Y. Myozyo and other members of the research group "Multiparticle Productions" organized by the Research Institute for Fundamental Physics, Kyoto University, in 1971.

Appendix

Notation and kinematics of inclusive reactions and triangle plot

We summarize our notation and explain the kinematics of inclusive reaction. Relations among kinematical variables may be easily understood on the triangle

plot explained here.

We denote the four momenta of particles a, b and c in the reaction $a+b\to c+X$ as P_a, P_b and q, respectively. Similarly to the two-body kinematics, the invariant variables can be defined as follows:

$$s=(P_a+P_b)^2,$$

$$t=(P_a-q)^2,$$

$$u=(P_b-q)^2$$

and

$$s+t+u=m_a^2+m_b^2+m_c^2+M_X^2, \qquad (A\cdot 1)$$

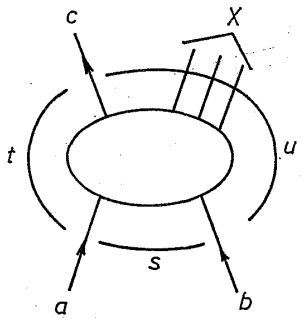

Fig. 17. Definition of variables for the reaction $a+b\to c$ +anything (X).

where M_X denotes the missing mass, and m_a, m_b and m_c are the masses of the particles a, b and c, respectively (see Fig. 17). The variables t^* and u^* used in § 3, are defined as

$$t^*\equiv 2P_a\cdot q=m_a^2+m_c^2-t\,,$$

$$u^*\equiv 2P_b\cdot q=m_b^2+m_c^2-u\,.$$

These variables are more convenient than t and u, because they are positive and not explicitly depend on the masses of the incident particles m_a and m_b. From Eq. (A·1) we have the constraint

$$t^*+u^*+M_X^2=s+m_c^2. \qquad (A\cdot 2)$$

We may consider that at high energies, the large value of s is divided into t^*, u^* and M_X^2. Therefore, physical region for the process $a+b\to c+X$ is restricted in a triangle in (t^*, u^*) plane, as shown in Fig. 18.

On the other hand, Feynman's variable

$$x=2q_{\parallel}/\sqrt{s}$$

and $q_\perp^2$ are frequently used as a set of scaling variables, where $q_{\parallel}$ and $q_\perp$ are the longitudinal and transverse momenta of the particle c in the center-of-mass system with the forward direction given by $\boldsymbol{P}_a$. However, for the studies including large $q_\perp^2$ region, the set $(\bar{x}, q_\perp^2)$ may be more convenient, where

$$\bar{x}\equiv 2\omega_q/\sqrt{\ }=\sqrt{x^2+\frac{4(q_\perp^2+m_c^2)}{s}}\,.$$

Here ω_q is the C.M. energy of the particle c. These variables are related to s, t^*, u^* and M_X^2 as follows:

$$\bar{x}\simeq\left(1-\frac{M_X^2}{s}\right)+\frac{m_c^2}{s}$$

$$\simeq\frac{t^*+u^*}{s}, \qquad (A\cdot 3)$$

$$q_\perp^2 + m_c^2 \simeq \frac{t^* u^*}{s} . \qquad (A\cdot 4)$$

Conversely, t^* and u^* are expressed as

$$t^* \simeq \frac{s}{2}(\bar{x} - x) + m_a^2 \bar{x}$$

$$\simeq \frac{q_\perp^2 + m_c^2}{(\bar{x} + x)/2} + m_a^2 \bar{x} , \qquad (A\cdot 5)$$

$$u^* \simeq \frac{s}{2}(\bar{x} + x) + m_b^2 \bar{x}$$

$$\simeq \frac{q_\perp^2 + m_c^2}{(\bar{x} - x)/2} + m_b^2 \bar{x} . \qquad (A\cdot 6)$$

In the scaling limit, $O(m_i^2/s)$ is neglected and we have Eq. (3·2) in § 3.

In the triangle plot of t^*, u^* and M_X^2 in Fig. 18, the vertical and horizontal lines correspond to constant x and $\bar{x}$, and a line with constant $q_\perp^2$ is represented by a hyperbola, for sufficiently large s. In Fig. 19 the Peyrou plot by $(q_\parallel, q_\perp)$ is exhibited for comparison, where $\bar{x}$ = constant gives a circle and the physical region is restricted within the circle $\bar{x} \lesssim 1$. In terms of t^* and u^*, the line with $q_\perp^2$ = constant implies small t^* or u^* for $x > 0$ or $x < 0$, but the situation at $x \approx 0$ is very complicated.

The invariant cross section $\omega_q (d\sigma/d\boldsymbol{q}) \equiv \rho$ is a function of three independent variables such as $(s, x, q_\perp^2)$, and the scaling contribution is characterized as an s independent part of ρ. In general, we have the following expressions:

$$\rho = \frac{\bar{x}}{\pi} \frac{d^2\sigma}{dx dq_\perp^2}$$

$$\simeq \frac{1}{\pi} \frac{d^2\sigma}{d\bar{x} dt^*} .$$

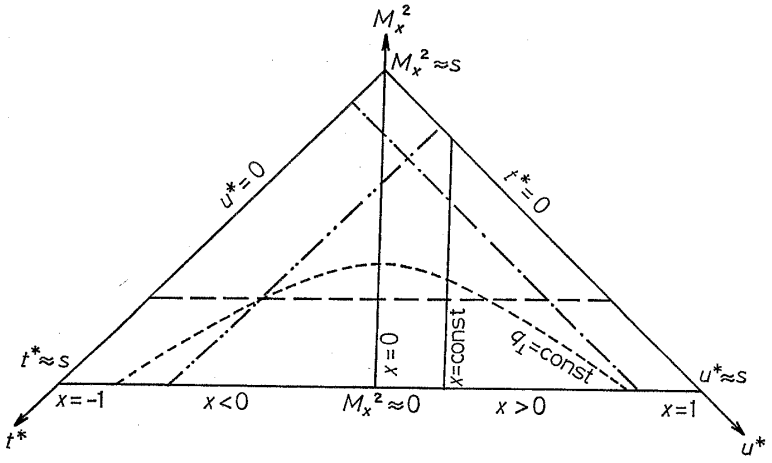

Fig. 18. The triangle plot by taking t^* and u^* as orthogonal coordinates.

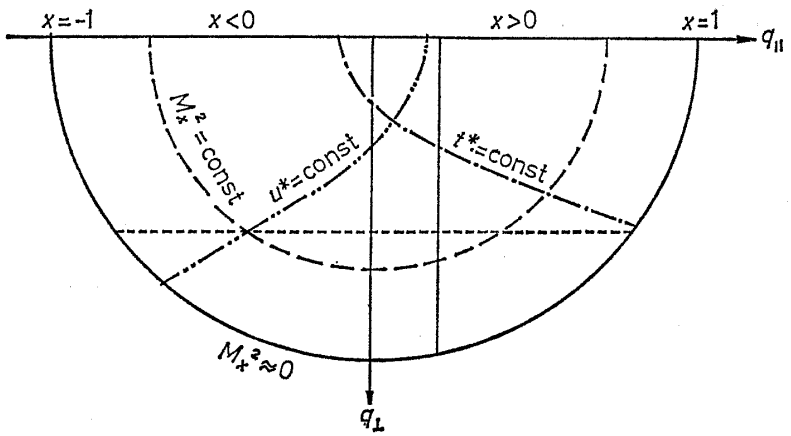

Fig. 19. The Peyrou plot by taking $q_{\parallel}$ and $q_{\perp}$ as orthogonal coordinates.

The missing mass distribution is related to ρ as

$$\frac{d^2\sigma}{dt^* dM_X} \simeq 2\pi \frac{M_X}{s}\rho \,.$$

References

1) J. Benecke, T. T. Chou, C. N. Yang and E. Yen, Phys. Rev. **188** (1969), 2159.
2) R. P. Feynman, Phys. Rev. Letters **23** (1969), 1415.
3) J. V. Allaby et al., CERN preprint (CERN 70-12).
4) J. C. Vander Velde, Phys. Letters **32B** (1970), 501.
   N. F. Bali, Lowell S. Brown, R. D. Peccei and A. Pignotti, Phys. Rev. Letters **25** (1970), 557.
   H. Bøggild, K. H. Hansen and M. Suk, Nucl. Phys. **B27** (1971), 1.
5) A. H. Mueller, Phys. Rev. **D2** (1970), 2963.
6) M. Imachi, T. Matsuoka, K. Ninomiya and S. Sawada, Prog. Theor. Phys. **40** (1968), 353.
   T. Matsuoka, K. Ninomiya and S. Sawada, Prog. Theor. Phys. **42** (1969), 56.
   H. Noda and F. Toyoda, Prog. Theor. Phys. **45** (1971), 1634.
   M. Imachi, T. Oroguchi, S. Otsuki and F. Toyoda, Prog. Theor. Phys. **45** (1971), 1849.
7) A. Kobayashi, T. Matsuoka, K. Ninomiya and S. Sawada, Prog. Theor. Phys. **45** (1971), 403.
   K. Ghoroku, Y. Myozyo and H. Noda, Prog. Theor. Phys. **45** (1971), 1695.
8) C. E. DeTar, C. E. Jones, F. E. Low, J. H. Weis, J. E. Young and Chung-I Tan, Phys. Rev. Letters **26** (1971), 675.
   N. F. Bali, A. Pignotti and David Steele, Phys. Rev. **D3** (1971), 1167.
9) J. Iizuka, Prog. Theor. Phys. Suppl. Nos. 37 and 38 (1966), 21.
10) K. Ghoroku, Y. Myozyo and H. Noda, Prog. Theor. Phys. **46** (1971), 820.
11) P. H. Frampton and P. G. O. Freund, Nucl. Phys. **B24** (1970), 453.
12) A. K. Wroblowski, *15th International Conference on High Energy Physics, Kiev, 1970.*
13) J. Bartke et al., Nuovo Cim. **29** (1963), 3118.
14) J. D. Hansen, W. Kittel and D. R. O. Morrison, Nucl. Phys. **B25** (1971), 605.
15) W. Ko and R. L. Lander, Phys. Rev. Letters **26** (1971), 1064.
16) J. V. Allaby et al., Phys. Letters **34B** (1971), 435.
17) E. W. Anderson et al., Phys. Rev. Letters **25** (1970), 699.
18) E. W. Anderson et al., Phys. Rev. Letters **16** (1966), 855.
19) J. Wang and L. Wang, Phys. Rev. Letters **26** (1971), 1287.

20) L. Caneschi and A. Pignotti, Phys. Rev. Letters **22** (1969), 1219.
See also C. Risk and J. H. Friedman, Phys. Rev. Letters **27** (1971), 654.
21) F. Binon et al., Phys. Letters **30B** (1969), 506.
22) N. F. Bali, A. Pignotti and David Steele, Phys. Rev. **D3** (1971), 1167.
23) W. Ko and R. L. Lander, Phys. Rev. Letters **26** (1971), 1284.
24) J. V. Beaupre et al., Nucl. Phys. **B30** (1971), 381.
25) H. Satz and D. Schildknecht, Phys. Letters **36B** (1971), 85.
26) J. Iizuka, M. Kobayashi and H. Nitto, Prog. Theor. Phys. **45** (1971), 482.
27) J. V. Allaby et al., Phys. Letters **33B** (1970), 429.

Note added in proof:

1. The three categories of production mechanism and all the types of the URD for inclusive reactions are extensively discussed in our subsequent paper submitted to Prog. Theor. Phys., "Interrelation between Exclusive and Inclusive Reactions". There, the reduction rule of urbaryon lines is formulated, which is implicitly assumed in the present paper.

2. The approach with energy increase to asymptotic distributions of the $H\otimes P$ and $H\otimes P$ types are investigated in our another paper, "Production Rates and Distinctive Components of Single-Particle Distributions" (submitted to Prog. Theor. Phys).

3. After submittion of the present manuscript, we have become awared that the $(1-|x|)$ power form of the single-particle spectrum outside the region $1\,\mathrm{GeV}\ll M_x^2\ll s$ was independently discussed by a few groups from different viewpoints. Based on the limiting fragmentation picture,[1] the power form is discussed by T. T. Chou, Phys. Rev. Letters **27** (1971), 1247. There, the value of the power is only determined phenomenologically. The effective trajectories in the triple-Regge parametrization for $pp\to cx$ are computed by two groups; M-S. Chen, L-L. Wang and T. F. Wang, BNL preprint (1971), G. Ranft and J. Ranft, Dubna preprint E2-6031 (1971). The results in these computations are consistent with our scheme in which the power is given by the rearranged urbaryon number.